Journal of Harbin Engineering University
ISSN: 1006-7043
Vol 45 No. 2
February 2024

COVID Detection from Multimodal Images Using ELM and UNET

[1]V L Nisha, [2]D Menaka
[1] Research Scholar, Department of Electronics and Communication Engineering, Noorul Islam Centre for Higher Education, Kumaracoil, India
[2] Associate Professor, Department of Electronics and Instrumentation Engineering, Noorul Islam Centre for Higher Education, Kumaracoil, India
Email: [1]nishavijayachandran@gmail.com, [2]menakaberita@gmail.com

Abstract

Coronaviruses are serious illnesses that affect both people and animals. Currently, the novel COVID-19 coronavirus is rapidly spreading over the world, putting billions of people's health. The majority of COVID-19 patients had a lung infection, according to clinical examinations. Computed Tomography (CT) is an effective imaging tool for identifying lung disorders which can have more detailed information about chest region. Chest X-ray is more widely available due to its faster imaging time and lower cost. Deep learning, one of the most effective AI technologies, helps radiologists to analyze vast numbers of chest images, which is critical for rapid and reliable COVID-19 screening. The goal of this project is to create a new deep anomaly detection model that can be used quickly, reliable screening of COVID-19 from CT and X-Ray Images. Here, to create the segmentation map, UNET is used after training with standard database of CT and X-ray images of COVID effected peoples. To classify normal, COVID or pneumonia, Extreme Learning Machine (ELM) is used with features such as center symmetric local binary pattern (CSLBP), shape features and arithmetic features. To improve the performance, image denoising, smoothing, and normalization techniques are used in the pre-processing stage. To evaluate the performance, sensitivity, specificity, accuracy, and precision statistical measures were utilized. This work achieved a maximum accuracy of 99.96%. The results suggest that this work performs better than conventional covid classification works.

Keywords: *COVID-19, Pneumonia, Deep Learning, Image Smoothing, Extreme Learning Machine, UNET, Center Symmetric Local Binary Pattern (CSLBP), Shape Features, Arithmetic Features.*

1. Introduction

The new Coronavirus (COVID-19) is an acute, fatal disease that began in China's Wuhan province in December 2019 and has since expanded worldwide. Because no effective treatment has been established, the COVID-19 epidemic has been of significant worry to the medical world. COVID-19's biologic architecture is a positive-oriented single-stranded RNA-type, and the condition is difficult to treat owing to its mutating nature. Medical professionals all throughout the globe are working hard to develop an appropriate cure for the condition. COVID-19 is the leading cause of mortality in the world today, with big outbreaks in the worldwide. Coronaviruses come in a variety of forms, and they're typically seen in animals. People with compromised immune systems may die as a result of the infection. COVID-19 is spread mostly through personal contact between people [1].

Artificial intelligence (AI) has recently been increasingly employed to speed up biological research. AI has been applied in a variety of

applications, including picture detection, data categorization, and image segmentation, using deep learning methodologies. People who are infected with COVID-19 may get pneumonia as a result of the virus's ability to move to the lungs. Many deep learning projects have employed chest X-ray image data to identify the condition, and the results have been promising.. [2].

When CT scans or X-Rays are used to identify COVID-19 symptoms in the lower lungs, the accuracy is greater than when RT-PCR is used. In certain cases, RT-PCR tests may take the role of CT scans and X-ray investigations. They are unable to adequately address the issue owing to the relatively limited number of radiologists compared to new residents, as well as the high incidence of re-examinations of ill people who want to know how their health is going. The procedure's speed must be enhanced to accommodate the limits of CT scans and X-rays while also benefiting radiologists. Artificial intelligence (AI) tools may be integrated into contemporary diagnostic systems to do this. The objective is to reduce the time and effort required to do CT scans and X-rays on COVID-19-positive patients, as well as to measure the rate of disease progression [3].

Deep Learning approaches have exploded in popularity in recent years, drastically altering the landscape of numerous academic disciplines. When deep learning algorithms are utilized on image data sets including retina pictures, chest X-rays, and brain MRI, they produce promising results with a higher accuracy percent. X-ray machines are commonly used in hospitals to scan various human organs and provide more inexpensive and faster results. The manual interpretation of diverse X-ray images is usually performed by a trained radiologist. If you train those collected images using deep learning as a data scientist, you may greatly assist medical specialists in spotting COVID-19 patients. This should benefit underdeveloped nations where an X-ray facility is accessible but an expert is still a pipe dream [4].

There has been a slew of accomplishments in COVID-19 detection since the deep convolution neural network technology attained an extraordinary edge in image processing. The CXRadiographs probable imaging biomarkers and built a deep neural network for COVID-19 CXR image interpretation using a patch-based CNN technique with a minimal number of trainable parameters and few training data [5].

This work proposes a new technique to improve the accuracy of COVID detection using multiple feature extraction followed by feature position and weight optimization to increase the classification accuracy. The following features are extracted: CSLBP, Arithmetic function and Shape feature, followed by the training and testing phase. Finally, the dataset is evaluated for performance, accuracy, sensitivity, specificity, precision, and kappa.

The remainder of the paper is laid out as follows: The connected works are presented in Section II. In Section III, the proposed approach is explained. Section IV, discuss experiments and analyses. Section V, concludes the work.

2. Related work

In summary, the current relevant works are reviewed given the previously large number of similar COVID detection and classification works in terms of feature extraction and combined effect.

Aras M. Ismael proposed profound element extraction, calibrating of pre-prepared Convolutional Neural Networks (CNN), and start to finish preparing of a fabricated CNN model were used to distinguish COVID-19 and ordinary chest X-beam pictures. Profound CNN models were utilized to remove profound attributes. Profound elements including Linear, Quadratic, Cubic, and Gaussian were characterized utilizing Support Vector Ma-

chines (SVM) classifiers. The fine-tuning approach also uses pre-trained deep CNN models. This work proposes a novel CNN model with end-to-end training. The study's success was assessed by the accuracy of its categorisation. Deep learning can recognise COVID-19 from X-ray pictures of the chest, according to the research. The deep features obtained using the ResNet50 model and SVM classifier utilising the function of Linear kernel had the highest accuracy score of all the results, with 94.7 percent accuracy [6].

Changjian Zhou et al. proposed using a combination of image regrouping and ResNet-SVM to analyze COVID-19 chest X-ray pictures. The lung region was segmented and separated into little parts from the original chest X-ray pictures, The little fragments of the lung area were then randomly reassembled into a normal picture. The regrouped images were also delivered to the deep residual encoder block, which extracted characteristics from the images after they were regrouped. Finally, the features were loaded into a support vector machine, which was used to recognise the objects. Because the visual attention was introduced in a novel way, the COVID-19 properties were able to be emphasised without being distracted by forms, ribs, or other distracting elements. In the experiments, it was discovered that the proposed technique surpasses existing COVID-19 detection models by obtaining 93 percent accuracy without the need for a large quantity of training data. [7].

Ali Narin et al. proposed for pre-trained convolutional neural network-based models for coronavirus pneumonia detection utilising chest X-ray radiographs (ResNet50-101-152-Inception-ResNetV3) have been suggested. Four classes of COVID-19 classifications were used using five-fold cross-validation (normal/healthy, viral/bacterial pneumonia). Among the four models examined, the pre-trained ResNet50 model had the best classification performance [8].

Linda Wang et al. proposed to recognise COVID 19 from Chest X-Ray pictures, COVID Net uses a deep CNN (DCN). COVID Net was released in 2008. Examine how COVID Net leverages explainability to build predictions, not just to better understand COVID cases, but also to aid doctors in better screening, and to audit COVID Net responsibly and openly to verify it is making conclusions based on relevant information from CXR pictures. [9].

Emtiaz Hussain et al. proposed a new CNN model called CoroDet that uses raw chest X-ray and CT scan data to identify COVID-19 automatically. Corot was designed to be a reliable diagnostic tool for two-class (COVID and Normal), three-class, and four-class classifications [10].

However, the above-mentioned methods have merits and demerits. The main disadvantage of the previous works is computation time and accuracy. The main objectives of this work are

1. To increase the accuracy of the classification.
2. Detect COVID-19 from chest CT and X-ray images with sufficiently high sensitivity, enabling fast and reliable screening.
3. To reduce the complexity of COVID-19 diagnosis process from X-ray and CT images.

The details of the implementation of the proposed work are given below sections.

3. Proposed Method COVID-19 Detection from CT and X-ray Images Using UNET and ELM

3.1. Block diagram

Fig.1. shows COVID detection from CT images using multiple feature extraction with ELM. This work, consists of four framework components: Image preprocessing, segmentation, Feature extraction network training, and classification, also, data segmentation

which plays an important role in this classification framework can be described and analyzed.

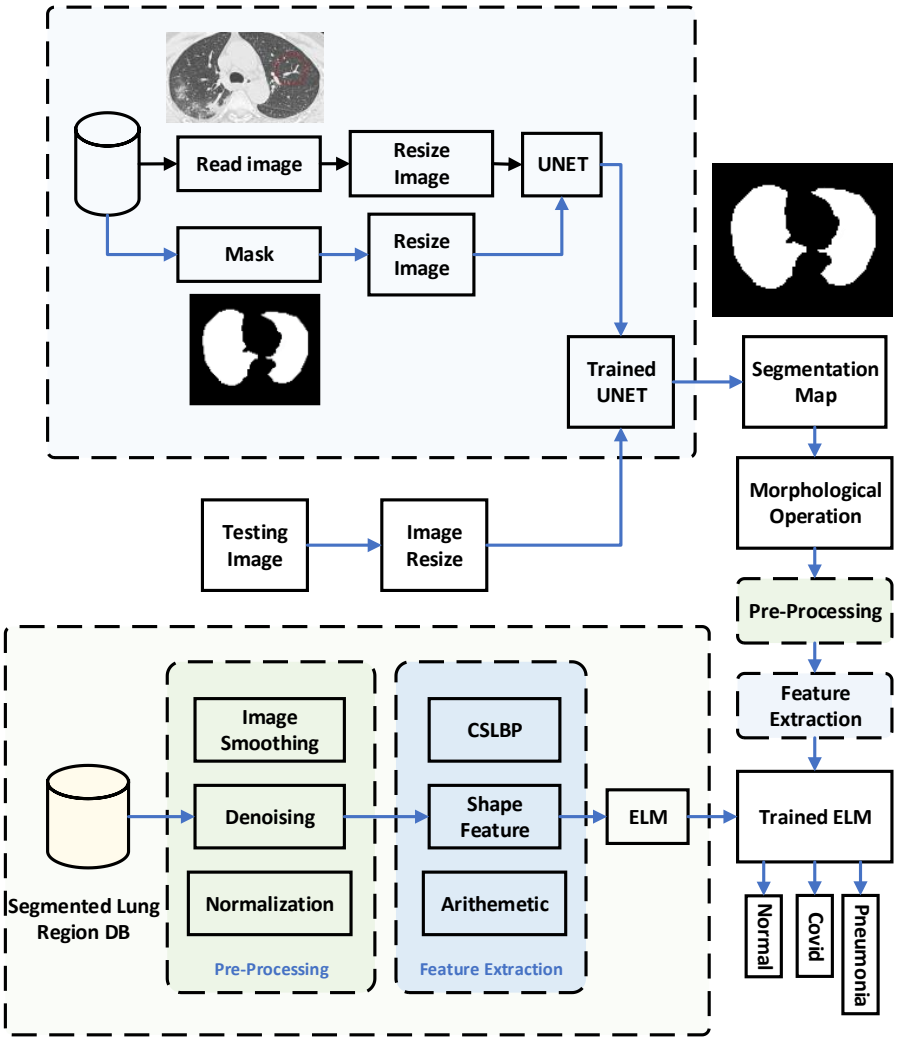

Fig.1. Block diagram for COVID detection using multiple feature extraction with ELM

3.2. *UNET Architecture*

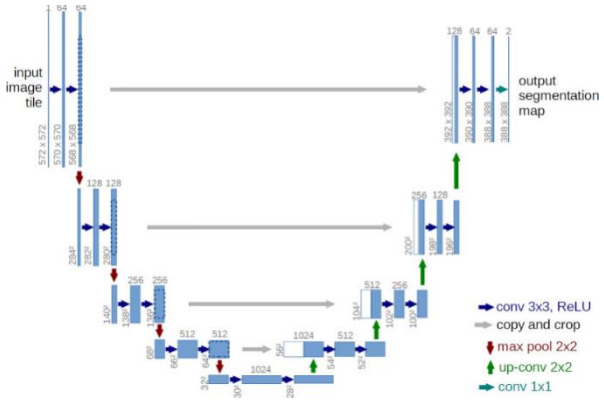

Fig.2. UNET architecture

The process of segmentation is accomplished by the use of an encoder-decoder neural network, commonly known as a UNET (unidirectional neural network). Performing a transposed convolution operation (deconvolution) on the information acquired in the decoder area of the network allows one to decode information from the latent space, therefore revealing previously hidden information. As a consequence of the procedure, a picture segmentation mask is created for the image.

With the exception of the encoder section, the remaining phases are identical to those used in the encoder portion of the programme. While looking at these two frameworks, one of the primary distinctions is the use of skip-associations to move data

from the suitable high-goal levels of the encoder to the relating high-goal layers of the decoder. Among UNET and the basic encoder-decoder worldview, which might empower the organization to better catch minute subtleties that are available in high-goal. This organization's plan is partitioned into two segments: contractive and expansive. The con-tracting approach, which follows ReLU layers, consists of numerous convolution patches with size 3x3 filters and uni-ty strides in both directions. This route takes the most important properties from the input and returns a feature vector of a predetermined length.

The second route copies and crops data from the contractive path, as well as up-convolutions data from the feature vector, and then employs numerous techniques to build an output segmentation map. The UNET architecture is seen in Figure 2. The operation that connects the first and second pathways is a key feature of this system. This connection allows the network to get very precise data from the contractive route, resulting in a segmentation mask that is as near to the intended output as feasible.

3.3. Image Segmentation

Segmentation is the division of an image into multiple parts with similar attributes or some similarities. Single-pixel sections are uncommon in segmentation

maps, which normally consist of several linked components [11-13]. It was found that embedding an express normalization term in the preparation misfortune work consider-capably raises the association prerequisites for favorable to projected division regions, permitting our segmentation model to pro-duce division maps with connected parts of wanted sizes. It's worth noting that UNET when educated starting from the earliest stage, may gain a portion of these ways of behaving certainly from preparing infor-mation.

3.3.1. Binary Dilation

In mathematical morphology, a binary image is considered as a subset of a Euclidean space R^dor the integer grid Z^d for some dimension d. Assume E is a Euclidean space or an integer grid, A is a binary picture in E, and B is a structuring element that is a subset of R^d. The dilatation of A by B is calculated as follows:

$$A \oplus B = \bigcup_{b \in B} A_b \tag{1}$$

where $A_b$is the translation of A by b.

3.4. Preprocessing

In the image preprocessing phase normaliza-tion, image enhancement, edge sharpening techniques are applied.

3.4.1. Image denoising

The Bayesian thresholding is proved to be one of the most efficient denoising formal-ism. For a white Gaussian noise, the thresh-old given by its optimal:

$$T_\beta(\sigma_X) = \frac{\sigma^2}{\sigma_X} \tag{2}$$

3.4.2. Normalization

Normalization is a procedure that changes the depth of pixel intensity esteems. Normal-ization is in some cases called contrast ex-tending or histogram extending. In progres-sively broad fields of information processing, for example, advanced signal handling, it is called unique range development.

Let us consider an n image with intensity range Min and max $I: \{X \subseteq R^n\} \rightarrow \{Min, \dots, Max\}$ normalization converts the image I into a new image $I_N = \{X \subseteq R^n\}\{newMin, \dots, newMax\}$ with intensity ranges from newMin to newMax. The Gray image normalization is performed by the equation

$$I_N = (1 - Min)\frac{newMax - newMin}{Max - Min} + newMin \tag{3}$$

3.4.3. Image smoothing

To reduce noise, the picture is blurred. As a result, the picture is smoothed first using a Gaussian filter. The suggested approach employs a 55 Gaussian template and the original image to weigh the neighborhood. When processing and extracting 55% neighborhood, designate any point (x, y) of the picture as the center. The weighted neighborhood might be expressed as follows:

$$I_a(x,y) = \frac{1}{5x5}\sum_{i=-2}^{2}\sum_{j=-2}^{2} I(x+i,y+j)xM(2+i,2+j) \quad (4)$$

where x=1,2,...,m; y=1,2,...,n; I(x,y) is the actual sub-pixel image's value, M is the Gaussian template, and $I_a(x,y)$ is the smoothed image's pixel value

3.5. Feature Extraction

Using five independent feature selection techniques CSLBP, SIFT, SURF, and Arithmetic high-level features with varying scales are retrieved from the segmented pulmonary areas in this stage. Because the re-trieved attributes serve as the foundation for categorising the COVID-19, the classification approaches exhibited low classification accuracy. There is unanimity that no one function performs flawless-ly since each feature has its own set of constraints.

3.5.1. CSLBP

It computes the histogram of the CSLBP operator, which is an extension of the LBP operator. Using CSLBP is useful for transforming photos that are both light and dark in appearance. Thus, the CSLBP histogram is extraordinarily long because of this factor. Please keep in mind that it is used as a description for a critical point in the document. Calculate a local patch around the key points, and then compute the CSLBP descriptor based on the key points and the local patch.

The CSLBP descriptor may be calculated using the follows

$$CSLBP_{r,p} = \sum_{i=0}^{\frac{p}{2}-1} f\left(\left|g_i - g_{i+\frac{p}{2}}\right|\right)2^i,$$
$$f(x) = \begin{cases} 1 & if\ x \geq \tau \\ 0 & otherwise \end{cases} \quad (5)$$

Where r denotes circle radius, p denotes counts of sampled points in the circle, W denotes slight threshold used for limit this same among center-symmetric pairs of pixels, g_i and $g_{i+p/2}$ denotes the gray-scale values of center-symmetric pairs of pixels, respectively.

3.5.2. Speeded-Up Robust Features (SURF)

Because of its strong properties, such as size invariance, translation invariance, illumination invariance, contrast invariance, and rotation invariance, the SURF method is used to recognize objects in photos captured under various extrinsic and intrinsic conditions.

$$S(x,y) = \sum_{i=0}^{x}\sum_{j=0}^{y} I(i,j) \quad (6)$$

3.5.3 Scale-Invariant Feature Transform (SIFT)

To build a "feature description" of a thing, you may extract interesting locations on any object in an image. This description, which was derived from a training picture, may be used to identify an object in a test image that includes a variety of other items. The properties gained from the training picture must be identifiable even under variations in image size, noise, and brightness in order to perform reliable identification. These spots are most often visible in high-contrast portions of the image, such as around the edges of objects. The SIFT feature descriptor can reliably recognise objects even amid clutter and partial occlusion since it is invariant to uniform scaling, orientation, and illumination changes, as well as partly invariant to affine distortion.

3.5.4 Arithmetic Feature

3.5.4.1 Standard Deviation (SD)

The SD as a calculation of the variation in a distribution of values throughout a range of values over a period of time. An extremely low SD suggests that values are frequently set as means, whereas an extremely large SD shows that values are evenly spread across a wide range of values.

$$s = \sqrt{\frac{1}{N-1} \sum_{i=1}^{N}(x_i - \bar{x})^2} \quad (7)$$

These observed values of a sample items are represented by the variables {x1, x2…xn} where $\bar{x}$ the mean of these observations is; and N is the total number of observations in the sample.

3.5.4.2 Mean

The mean of a collection of observed data, according to the definition, is equal to the sum of all numerical values for each observation divided by the total number of observations in the collection. The arithmetic means of a set of numbers x_1, x_2, ..., x_n is typically denoted by $\bar{x}$, n is the number of items in the sample in follows

$$\bar{x} = \frac{1}{n} \left(\sum_{i=1}^{n} x_i\right) = \frac{x_1 + x_2 + \cdots + x_n}{n} \quad (8)$$

3.5.4.1. Kurtosis:

It is a measure of how "tailed" a probability distribution with respect to a real-valued random variable is in probability theory and statistics. Kurtosis like skewness, is a probability distribution characteristic that specifies overall shape of a probability distribution as well as the techniques for estimating it from a sample of the population. It is also the fourth standardized instant, and it is defined as

$$\text{Kurtosis[X]} = \text{E}\left[\left(\frac{X-\mu}{\sigma}\right)^4\right] = \frac{E[(X-\mu)^4]}{(E[(X-\mu)^2])^2} = \frac{\mu_4}{\sigma^4} \quad (9)$$

where μ_4 is the fourth central moment and σ is the standard deviation. K denotes the kurtosis.

3.5.4.3 Skewness

According to probability theory and statistics, the skewness of a real-valued random variable's probability distribution with respect to its mean is a measure of the asymmetry of the probability distribution with respect to its mean. The skewness of the standardized moment $\tilde{\mu}_3$ defined as in Eq.(10)

$$\tilde{\mu}_3 = E\left[\left(\frac{X-\mu}{\sigma}\right)^3\right] = \frac{\mu_3}{\sigma^3} = \frac{E[(X-\mu)^3]}{(E[(X-\mu)^2])^{3/2}} = \frac{k_3}{k_2^{3/2}} \quad (10)$$

3.5.4.4 Moment

The concept of a moment is used in a variety of areas, including mechanics and statistics. If the zeroth moment is represented as the entire probability, and first moment is represented as the anticipated value. The variance might serve as a representation of the second central moment. The skewness of the data can be represented by the third standardized instant. Furthermore, the kurtosis is represented by the fourth standardized moment. If a function represents a probability distribution, every zeroth moment may be represented by one, and the first moment can also be represented by one, and so on and so forth until the function reflects a probability distribution.

The n-th real-valued moment continuous function f(x) real variable about c value is defined in Eq.(11)

$$\mu_n = \int_{-\infty}^{\infty}(x-c)^n f(x)\ dx \quad (11)$$

3.6 Extreme Learning Machine (ELM)

The ELM is an unique learning algorithm for a feed-forward neural network with a single hidden layer (SLFN). The input weights and biases of ELM are selected at random in this technique, while the output weights are determined analytically.Weights of output are measured as shown in Eq.(12).

$$f_L(x) = \sum_{i=1}^{L} \beta_i h_i(x) = h(x)\beta \quad (12)$$

where $\beta = [\beta_1, ..., \beta_L]^T$ is the output weights vector between $h(x)$ is the output vector of the hidden layer, $h(x) = [G(a_1, b_1, x), \ldots, G(a_L, b_L, x)]$ is $G(a, b, x)$ a nonlinear piecewise continuous function, $\{(a_i, b_i)\}_i^L = 1$ randomly generated input values.

$$Sigmoid\ Function: G(a, b, x) = \frac{1}{1+exp(-(a.x+b))} \quad (13)$$

From the input layer to the hidden layer, go through the following steps., x is an sample of input, a is the value of weight, and b is the value of bias. The $\{a, b\}$ pair is generated by randomly. $\| H\beta - T \|^2$ and $\| \beta \|$ where H is the hidden layer output matrix;

$$\begin{bmatrix} h_1(x_1) & \ldots & h_L(x_1) \\ \vdots & \ddots & \vdots \\ h_1(x_N) & \ldots & h_L(x_N) \end{bmatrix}$$

During the application phase of ELM, the least-squares approach was utilised in place of the more traditional optimization methods.

$$\beta = H^{\dagger}T, \quad (14)$$

T is the tag matrix and $H^{\dagger}$ is the inverse of the hidden layer output matrix of Moore–Penrose generalized. $H = [h^T(x_1), \ldots, h^T(x_N)]^T N$ is The training sample was used to acquire the results. The Moore–Penrose generalized latent layer output matrix inverse's function is to minimize the L2 norms in this case of $\| H\beta - T \|$ and $\| \beta \|$. A regularization coefficient C is included in an optimization approach is used to improve the ELM's resilience and generalization capacity. Therefore, given a K kernel, the weight set is learned as:

$$\beta = \left(\frac{I}{C} + K\right)^{-1} T \quad (15)$$

In this job ends with the classifying step. In the classification procedure, there is a 10-fold cross validity. Fig.3. shows the ELM architecture

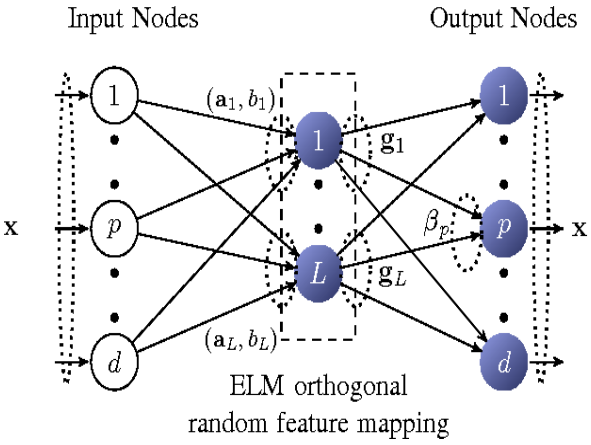

Fig.3. ELM architecture

4. Results and discussions

To evaluate the image classification using ELM, CT and X-ray images are collected from the Kaggle website. The average classification accuracy, which is the overall accurate classification score of all cell images utilized in the previous competition, is also determined for simplicity of comparison. MATLAB R2020b was used to complete this task using a machine with a Pentium(R) Dual-Core CPU E5800 @ 3.20GHz, 3192 Mhz, 2 Core(s), and 2 GB of RAM.

5. Dataset

The data collection utilised in this study is open source, and it presently has 337 pictures from 192 X-Ray scans of COVID-19 positive patients. Contributions are welcome to the photo archive, which is updated on a regular basis with new images. All of the photos, as well as the X-ray results, have been inspected and commented on exhaustively. The images came from a variety of places, including Radiopedia.org. The models were made using the Kaggle Chest X-Ray images dataset, which contains 5863 images of normal healthy adults. To classify these images, they were separated into four unique class values: This data set contains around 142 pictures of normal X-rays that were se-

lected from among them. Normal, Bacterial Pneumonia, and Viral Pneumonia, this data collection contains approximately 142 photos of normal X-rays, which were chosen from among them. This data set is further divided into two parts: training and testing. The training portion contains 75 percent of the data for training the proposed deep learning model, while the testing portion contains 25 percent of the data for testing purposes. Fig.4. shows the sample images

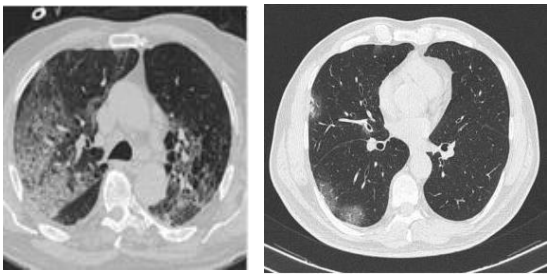

Fig.4. Sample CT images

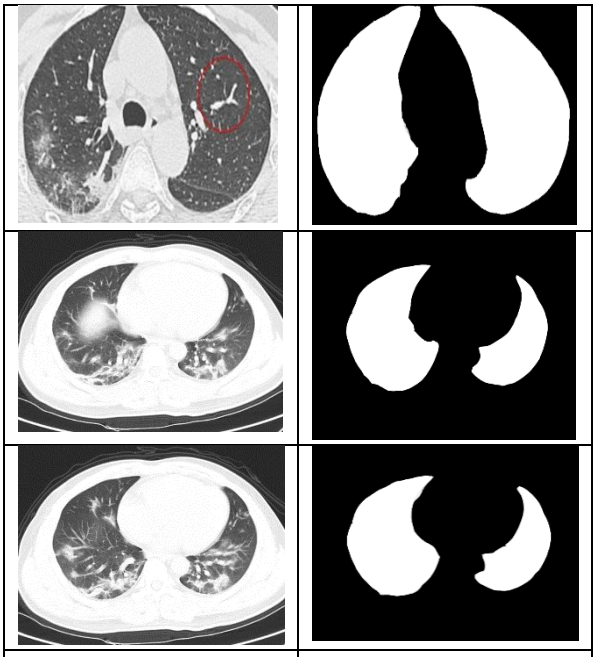

(a) *(b)*

Fig.5. Segmentation performed by using UNET, Fig.5. a. Input CT image, Fig.5. b. Segmentation map generated using UNET,

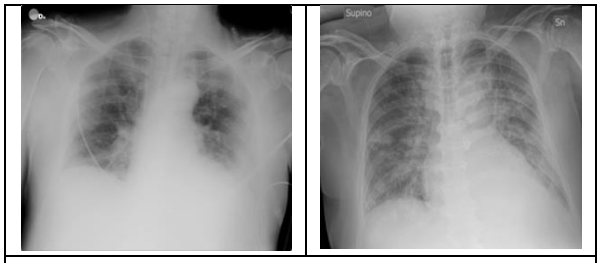

Fig.6. Sample chest X-ray images

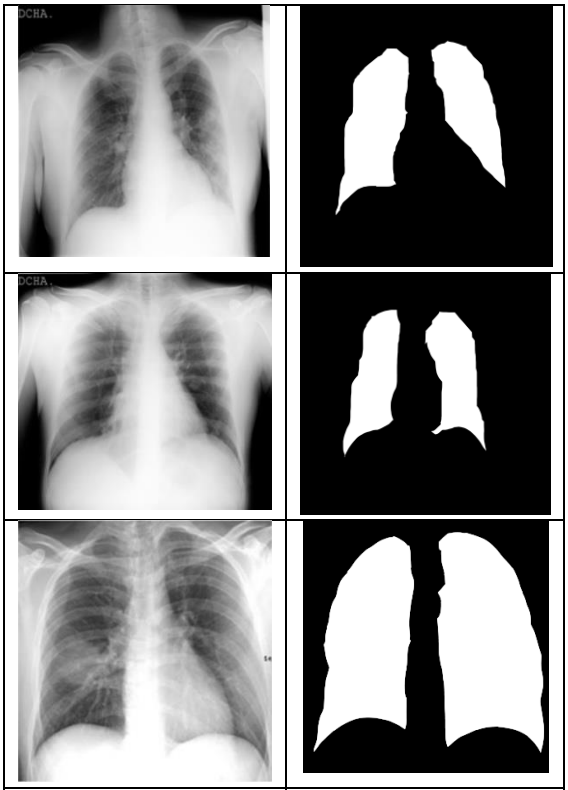

Fig.7. Segmentation performed by using UNET for chest X-ray images, Fig.7. a. Input X-ray image, Fig.7. b. Segmentation map generated using UNET for X-ray image,

5.1. Performance matrices

This work utilizes the most commonly used performance matrices to access this work. It consists of accuracy, sensitivity, specificity, precision, and kappa.

Accuracy (Ac), as defined above, is a mixture of all forms of observational error [14]; thus, high accuracy necessitates both high precision and high trueness. The method for calculating accuracy is as follows:

$$Accuracy = \frac{TP + TN}{TP + TN + FP + FN} \quad (16)$$

Where TP = True positive; FP = False positive; TN = True negative; FN = False negative

The sensitivity (Se) of a test refers to its ability to accurately distinguish patients who have the disorder [15-16]. It is often referred to as the True Positive Rate (TPR). Mathematically, it can be expressed as:

$$Sensitivity = \frac{No.of\ TP}{No.of\ TP + No.of\ FN} \quad (17)$$

Where TP = True Positives, FN = Number of False Negatives)

The ability of an examination to properly classify patients who do not have the disorder is referred to as specificity (Sp). It is sometimes referred to as the True Negative Rate (TNR).

$$Specificity = \frac{Number\ of\ TN}{Number\ of\ TN + Number\ of\ FP} \quad (18)$$

The Precision (Pr) is defined as:

$$Precision = \frac{TP}{TP + FP} \quad (19)$$

Where, TP=True Positive; FP=False Positive

Kappa coefficient (κ) is a formula for evaluating inter-rater durability components. It is widely accepted as a more robust statistic than a simple percent agreement calculation because it considers the likelihood of the agreement occurring by chance. The definition of κ is:

$$\kappa = \frac{p_o - p_e}{1 - p_e} = 1 - \frac{1 - p_o}{1 - p_e} \quad (20)$$

Where p_o The observed agreement among raters is the relative and p_e is the speculative likelihood of chance agreement.

5.2. Performance Analysis

Table.1 shows the training parameters of the proposed method. Table.2 compares the performance of accuracy, sensitivity, and specificity on the Kaggle CT, X-ray dataset. The size of the image increased also decreases the accuracy. Table.3. displays comparison with previous methods. Table.4. displays the relative accuracy performance depending on the testing and training ratio. When taking 50 percent training and testing 34 images it has an accuracy of 62.3, sensitivity of 65.9, and specificity of 61.6. Suppose take 60 percent images for testing and 40 percent images for training achieve 74.5 accuracies, 73.71 sensitivity, and 70.56 specificities. Finally get maximum accuracy of 96.1, the sensitivity of 96.4, and specificity of 95.3 for applying 70 percent testing images and 25 percent training images. Table.5. shows the Comparative performance based on the stages of COVID. Fig.5. shows the confusion matrix of the proposed method.

Table.1.
Training Parameters of the proposed method

Number of training images	1000
Number of testing images	700
Number of epochs	20
Iterations	1000

Table.2.
Performance of proposed method

Performance	X-ray	CT	X-Ray+CT
Accuracy	99.82	99.63	99.96
Sensitivity	98.2	98.46	98.41
Specificity	99.53	97.51	98.78
Precision	92.38	93.28	97.82

Table.3.
Comparison with previous methods

Method	Accuracy	Sensitivity	Specificity	Precision
[11]	87.02	85.35	92.18	89.96
[12]	99.4	99.3	99.2	98.12
[13]	98.97	89.39	99.75	97.77
[14]	89.50	87.00	88.00	92.19
[15]	92.64	91.37	95.76	96.71
This method	99.96	98.2	99.53	92.38

Table 4.
Comparative Performance of Based on The Ratio of Testing and Training Images

	Percentage (%)

Testing	50	60	75
Training	50	40	25
Accuracy	62.3	74.5	99.96
Sensitivity	65.9	73.71	96.4
Specificity	61.6	70.56	95.3

Table 5.
Comparative Performance of Based on The Stages of COVID

	Percentage (%)		
	Normal	Medium	Critical
Accuracy	99.42	99.46	99.19
Sensitivity	98.17	98.76	93.15
Specificity	93.76	93.43	98.18

Table 6.
Training and Validation performance of Image segmentation (UNET) concerning iteration

No of Epochs	TL	TA	VL	VA
25	0.5217	96.5	0.5112	96.251
30	0.4631	97.1	0.4421	97.058
35	0.4123	97.5	0.3912	97.563
40	0.3621	98.6	0.3325	98.321
45	0.2516	99.1	0.2351	99.101
50	0.1475	99.6	0.1523	99.261

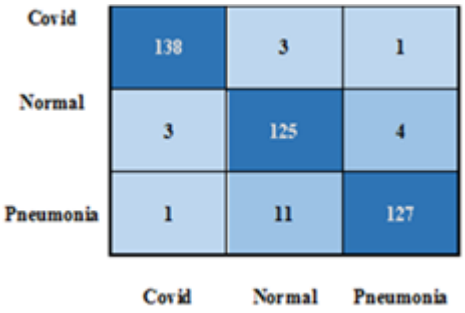

Fig.8. Confusion matrix of the proposed method

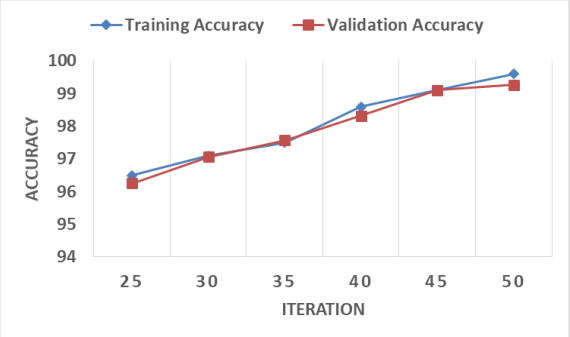

Fig.9. Validation and training Accuracy concerning the number of iterations

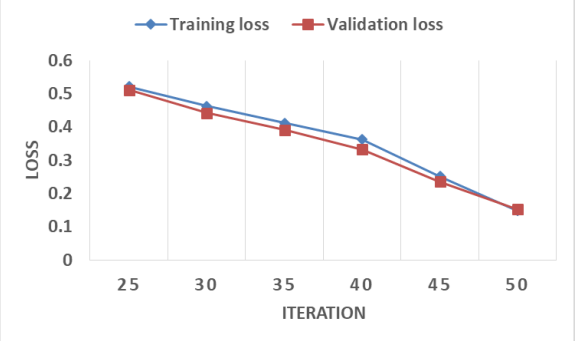

Fig.10. Validation and training loss concerning the number of iterations

6. Conclusion

In this work, a new technique is proposed to perform COVID-19 detection from CT and chest X-ray images. Initially, the segmentation map for the chest region is generated by using a trained UNET using a standard image database from the Kaggle website. The segmented chest region is further cropped and performed the pre-processing operation. In the pre-processing, image denoising, smoothing, and resizing are performed to improve the quality of post-processing. Multiple features such as CSLBP, shape, and arithmetic features of the cropped region are extracted and trained using ELM for further prediction of Normal, Covid, or pneumonia classes. This work achieved a maximum accuracy of 99.96 % which is prior when compared to conventional covid classification techniques.

Acknowledgement

This work uses deep learning for detection of Covid. AI is used in segmentation and classification sessions.

References

[1] Panwar, Harsh, P. K. Gupta, Mohammad Khubeb Siddiqui, Ruben Morales-Menendez, and Vaishnavi Singh. "Application of deep learning for fast detection of COVID-19 in X-Rays using nCOVnet." Chaos, Solitons & Fractals 138 (2020): 109944

[2] Civit-Masot, Javier, Francisco Luna-Perejón, Manuel Domínguez Morales, and Anton Civit. "Deep learning system for COVID-19 diagnosis aid using X-ray pulmonary images." Applied Sciences 10, no. 13 (2020): 4640.

[3] Jain, Rachna, Meenu Gupta, Soham Taneja, and D. Jude Hemanth. "Deep learning based detection and analysis of COVID-19 on chest X-ray images." Applied Intelligence 51, no. 3 (2021): 1690-1700.

[4] Haque, Khandaker Foysal, and Ahmed Abdelgawad. "A deep learning approach to detect COVID-19 patients from chest X-ray images." AI 1, no. 3 (2020): 418-435.

[5] Haghanifar, Arman, Mahdiyar Molahasani Majdabadi, Younhee Choi, S. Deivalakshmi, and Seokbum Ko. "Covid-cxnet: Detecting covid-19 in frontal chest x-ray images using deep learning." arXiv preprint arXiv:2006.13807 (2020).

[6] Ismael, Aras M., and Abdulkadir Şengür. "Deep learning approaches for COVID-19 detection based on chest X-ray images." Expert Systems with Applications 164 (2021): 114054.

[7] Zhou, Changjian, Jia Song, Sihan Zhou, Zhiyao Zhang, and Jinge Xing. "COVID-19 Detection based on Image Regrouping and ResNet-SVM using Chest X-ray Images." IEEE Access (2021).

[8] Narin, Ali, Ceren Kaya, and Ziynet Pamuk. "Automatic detection of coronavirus disease (covid-19) using x-ray images and deep convolutional neural networks." Pattern Analysis and Applications (2021): 1-14.

[9] Wang, Linda, Zhong Qiu Lin, and Alexander Wong. "Covid-net: A tailored deep convolutional neural network design for detection of covid-19 cases from chest x-ray images." Scientific Reports 10, no. 1 (2020): 1-12.

[10] Hussain, Emtiaz, Mahmudul Hasan, Md Anisur Rahman, Ickjai Lee, Tasmi Tamanna, and Mohammad Zavid Parvez. "CoroDet: A deep learning-based classification for COVID-19 detection using chest X-ray images." Chaos, Solitons & Fractals 142 (2021): 110495.

[11] Ismael, Aras M., and Abdulkadir Şengür. "The investigation of multiresolution approaches for chest X-ray image based COVID-19 detection." *Health Information Science and Systems* 8, no. 1 (2020): 1-11.

[12] Haritha, D., M. Krishna Pranathi, and M. Reethika. "COVID detection from chest X-rays with DeepLearning: CheXNet." In *2020 5th International Conference on Computing, Communication and Security (ICCCS)*, pp. 1-5. IEEE, 2020.

[13] Rai, Praveen, Ballamoole Krishna Kumar, Vijaya Kumar Deekshit, Indrani Karunasagar, and Iddya Karunasagar. "Detection technologies and recent developments in the diagnosis of COVID-19 infection." *Applied microbiology and biotechnology* 105, no. 2 (2021): 441-455.

[14] Alwashmi, Meshari F. "The use of digital health in the detection and management of COVID-19." *International Journal of Environmental Research and Public Health* 17, no. 8 (2020): 2906.

[15] Sethy, Prabira Kumar, and Santi Kumari Behera. "Detection of coronavirus disease (covid-19) based on deep features." (2020).

[16] Ni, Ling, Fang Ye, Meng-Li Cheng, Yu Feng, Yong-Qiang Deng, Hui Zhao, Peng Wei

et al. "Detection of SARS-CoV-2-specific humoral and cellular immunity in COVID-19 convalescent individuals." *Immunity* 52, no. 6 (2020): 971-977.